A computational study of structural and excitonic properties of chlorosomes

Li, X.

CHAPTER 5

Chirality versus Optical Responses of Chlorosomal Tube Aggregates: Highlighting the Role of Sample Preparation

Approaching the end of this thesis, I may become a bit more generic. Therefore, instead of solely considering tubes according to specific chiral angles, I systematically investigate the effect of chirality on the experimentally measurable optical properties. I do so by presenting i) the general protocol for constructing stable atomistic tube structures according to pre-defined chirality, which I apply ii) for the construction of chlorosomal tubes in the range [0°,180°), with an angular resolution of 5°. I note that the protocol under i) is more generally applicable for the construction of molecular assemblies of a chiral nature. In this short chapter, I employ the Frenkel treatment discussed in Charter 3 to tube assemblies to determine a 'phase diagram' of chirality versus optical spectra, in analogy to known phase diagrams in terms of thermodynamic variables. I considered structures obtained by the protocol substantiated further on, and that the considered range of angles covers all possible chiral tube angles for reasons of symmetry. Such *in silico* experiments allow us to clarify the optical fingerprints of chlorosomal tube aggregates and to obtain an improved understanding of the robustness of circular dichroism (CD) spectra measured in experiments.

This chapter is to be submitted as: *In Silico* Prediction of Chirality versus Optical Responses of Chlorosomal Tube Aggregates, 2020.

5.1. Introduction

Helical structures are particularly prevalent in biology, as exemplified by the helicity in proteins as well as in the molecules that encode proteins and are seen to encode most biological function and thus life itself — deoxyribonucleic acid or DNA — the structure of which was determined in the early 1950s.[159,160] Beside single helices formed through covalent bonds, like the ones in proteins and DNA, many structures display chiral or helical characteristics as a result of non-covalent interactions,[101,161] including the cell cytoskeleton,[162] myosin filaments,[163] bacterial flagella,,[164] and filamentous bacteriophage.[165] Yet, since the formation of quasi-2D helical motifs as a result of some sort of symmetry breaking is also frequently observed in synthetic systems and in specific phenomena therein, helicity is of a more universal significance.[166,167]

As an intriguing and sometimes functionally-relevant property of biological matter and some bio-inspired materials, helicity directly or indirectly relates to distinct and attractive mechanical, optical and other functional properties.[168–171] An example of particular interest are chlorosomes, *i.e.* tubular aggregates that are solely assembled from pigment molecules, which are recognized as the most efficient light-harvesting antennae found in nature,[15,16] and are rather unique in the finding that protein-based encoding of their light-harvesting function is essentially lacking. Inspired by chlorosomes, other large tubular molecular aggregates (TMA) formed by small molecules are attracting increasing attention in recent years for electronic and photonic applications.[28,48,125,172–180] In particular, some TMAs show extraordinary energy transport abilities.[50,181,182] Such structures are assembled, as noted earlier, from thousands of molecules that have been densely packed into a tubular geometry, having a diameter in the order of 10 nm and a length that may extend to hundreds of nanometers or even several micrometers.[28] In general, their structural organization is insufficiently characterized by experiments, owing to structural heterogeneity and the resulting lack of a distinct crystalline organization. More generally, the effect of supramolecular or tube chirality on the optical properties is still poorly understood.

In principle, we are able to reconstruct tube structures systematically and to probe corresponding optical properties by means of theoretical or numerical *in silico* experiments, and also to understand their relation towards extraction

of design parameters. In practice, however, it remains challenging to obtain atomistic structures of tube aggregates with a customized tube chirality, a challenge that seriously hinders such an *in silico* study.[51]

Here we demonstrate that, combining a new in-house packing code (CTubeGen)[1] and all-atom molecular dynamics (MD), we can effortlessly produce atomistic chlorosome tube structures with a pre-defined and customized tube chirality. This protocol is described in section 5.2.1. Besides for building the chlorosomes in this work, such a protocol may prove useful for generating other TMA systems. In addition, we use these structures to calculate optical spectra, including absorption, linear dichroism (LD), and circular dichroism (CD), for the full range of chiral vectors. The thus obtained chirality versus spectra 'phase-diagram' for the first time elucidates the relation between the overall tube chirality and the optical property of chlorosomes, resolving a long-standing issue how to explain different types of CD spectra observed for very similar chlorosomes. In particular, we show that the mystery of a mixture-type CD signal, which gave rise to explanation in terms of length-dependence, or a mixture of structures with different curving directions,[35,37,80] can be explained in terms of a single assembly with a particular chirality. We find that the shape of CD spectra changes abruptly when the chiral angle crosses into a different ranges, which may clarify this uncontrollable variation of CD spectra observed in experiments. Hence, it can be attributed to the preparation process: depending on the bacterial species or the chlorosome growth conditions, the chirality is not fully controlled, and even small changes in chirality may cause a distinct change of CD spectra.[35,88] We add that, besides optical properties, also other properties, *e.g.* mechanical properties, can be studied using these atomistic structures and MD simulation, see the next chapter.

[1] A software written in python, available in `chapter_5` folder at https://github.com/xinmeng2015/chlorosome_phd_thesis or https://doi.org/10.5281/zenodo.3674742

5.2. Results

5.2.1. The Protocol

Figure 5.1 and the following three steps outline the protocol that we developed for generating chiral structures with atomic resolution. In this study, we applied the protocol for the generation of chlorosome tubes starting from a *syn-anti* dimeric unit cells.

Stage 1, initial preparation. The goal of this stage is to generate a proper local packing, by equilibrating small planar aggregates. The molecular basis or composing unit of a given tube system has to be determined a priori. For chlorosomes, it is a *syn-anti* dimer of BChl pigments determined from a combination of solid-state NMR measurements and DFT calculation.[37] Next, one should select parameters in the force field based on the prior knowledge, *i.e*, the known molecular topology and chemistry. One should take great care of this procedure, since it is important for the accuracy of the MD simulations; we refer to Chapter 2 for details of our force field parameterization for BChl molecules. Next, it is easy to duplicate the composing unit according to the two-dimensional lattice parameters (a, b, γ) and generate small planar aggregates. If the thus formed structure turns out to be stable under MD simulation *in vacuo*, this stage is ready. If not, the lattice parameters (a, b, γ) should be tuned until a stable assembly is formed. Usually, input lattice parameters (a, b, γ) are available from the literature, for instance, from crystal diffraction measurements or DFT calculations. If not, one could perform 'brute-force' sampling, considering the limited point groups that are present in two dimensions.

Stage 2, tube packing. The goal of the second stage is to generate customized tube structures by molecular packing, making use of the information from the last stage. The new lattice parameters (a, b, γ) and the unit cell, which are selected from the stable assembly of stage 1, form the primary input to our packing code. This guarantees consistency at the level of the MD force field, which determines the stability of the structure in the following MD simulations, as well as a proper overall mass density. The packing code generates molecular tube structures in a highly customizable fashion. Variable properties include the total length of the tube, its curving direction, the tube radius, and the

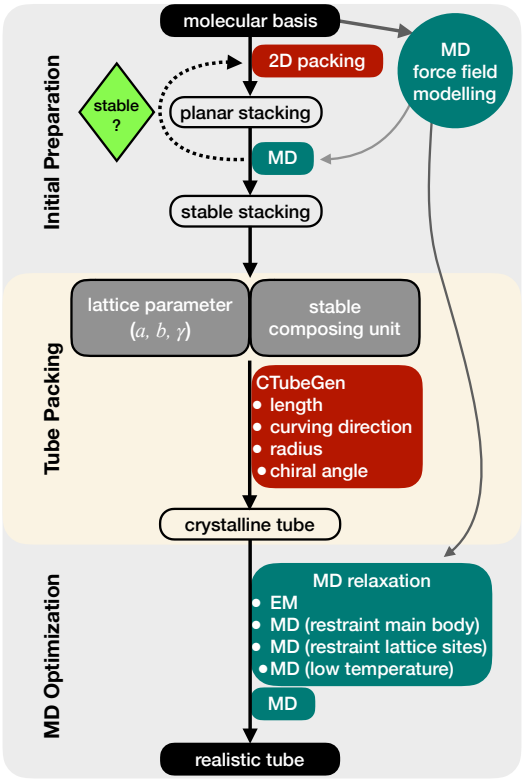

Figure 5.1: A schematic illustration of the protocol developed to obtain atomistic tube structures of chlorosomes.

chiral angle. The last two parameters define the chiral vector, which relates to the chiral indices (n_1, n_2) as $\mathbf{C} = n_1\mathbf{a} + n_2\mathbf{b}$. A key step is to convert the supramolecular chirality to the local twist angle α and rise distance h that is needed for a helical growth of composing units.[183,184]

By applying rotation (by an angle α) and translation (over a distance h) to a composing unit along both the **a** and **b** directions, starting from the base of the tube, we obtain a full tube structure. The algorithm details of our code is explained in the following subsection. It makes sense to visually consider the pre-packed tube structure, since distinct molecular overlap should be avoided. In particular, molecules with a ring topology may become interlocked with each other upon placement, an issue that cannot be resolved by simple relaxation.

Stage 3, MD optimization. The final stage aims at resolving stresses that may be present in the pre-packed regular structure,[51] and to introduce structural disorder on the level of classical MD. To this aim, we perform a set of MD simulations in a sequential fashion. First, we perform energy minimization (EM) by steepest descent to remove any distinct structural overlap that may cause numerical instability in MD. Next, we perform MD simulations with changing positional restraints to remove frustrations that may cause unfavorable structural defects. In our case, MD simulations with restraints on the head part (or heads) of all molecules aims at relaxing the conformations of the flexible tails. After removing these head restraints, only the positions of the Mg^{2+} ions, which relate directly to lattice sites, are restrained, allowing all other atoms in the head part to relax while maintaining a unit cell lattice. After this step, all position-restraints are removed, and we perform mild thermal annealing by unconstrained MD simulations at a reduced temperature of 50 K.

Finally, the structure is sufficiently equilibrated to perform unconstrained MD simulations in the target thermodynamic conditions, which, in our case, are at room temperature. We note that it is also possible to include solvent at this stage, in order to obtain a tube structure beyond the *in vacuo* condition. If so, it is also worthwhile to optimize the planar aggregates in the preferred solvent at stage 1.

5.2.2. The Algorithm of CTubeGen

Determination of chiral lattice and helix growth parameters

The pre-requisites:

- Select lattice parameters ($|\mathbf{a}| = a, |\mathbf{b}| = b, \gamma$) for the unit cell. For BChl *c* chlorosomes: $a = 1.48$ nm, $b = 0.98$ nm, $\gamma = 124.3°$ (see Chapter 2).
- A regular lattice on the tube can only be formed if the rolling or chiral vector $\mathbf{C} = n_1\mathbf{a} + n_2\mathbf{b}$, with n_1 and n_2 integer numbers that are often referred to as chiral indices.[185,186] Selecting n_1 and n_2 defines the tube radius $r = |\mathbf{C}|/2\pi$. For the purpose of illustration, we selected $n_1 = 30$ and $n_2 = 10$, equivalent to $r = 6.3$ nm. The corresponding chiral angle $\delta = \arccos(\mathbf{C} \cdot \mathbf{a}/(|\mathbf{C}| \cdot |\mathbf{a}|)) = 11.8°$.
- Align the unit cell by defining the x-axis along the **a**-direction and letting the plane spanned by **a** and **b** coincide with the x-z plane. Subsequently, perform a rotation in this plane to pre-orient **a** along the desired direction with a δ angle with the x-axis, as we set the **C** along the x-axis. For our case, the desired direction is along $(x, z) = (r \cdot sin(\alpha_a), -h_a)$, with α_a and h_a given below. Finally, translate the unit cell such that one of the Mg^{2+} ions is centered at $(0, 0, 0)$, and define the set of position vectors for all L atoms: $\mathcal{X}^0 = \{\mathbf{x}_l | l = 1, ..., L\}$.
- For $0° \leq \delta \leq 180°$, the rotational angle or twist between subsequent molecules growing along the **a** and **b** directions are given by:

$$\alpha_{\mathrm{a}} = \frac{360° \cdot a \cdot cos(\delta)}{|\mathbf{C}|}, \quad \alpha_{\mathrm{b}} = \frac{360° \cdot b \cdot cos(\gamma - \delta)}{|\mathbf{C}|} \tag{5.1}$$

  and the translational distance or rise for molecules growing along the **a** and **b** directions are given by:

$$h_{\mathrm{a}} = a \cdot sin(\delta), \quad h_{\mathrm{b}} = b \cdot sin(\gamma - \delta) \tag{5.2}$$

  where the subscript relates to the **a** or **b** direction. Since the signs of these variables depend on the way the tube is built, we will only consider absolute values. For $\delta = 11.8°$, the twists are $\alpha_{\mathrm{a}} = 13.1°$ and $\alpha_{\mathrm{b}} = 3.4°$ and rises $h_{\mathrm{a}} = 0.30$ nm and $h_{\mathrm{b}} = 0.91$ nm.

The corresponding geometrical representations can be found in Figure 5.2.

Tube building through a 2D helix growth

Our chlorosome tube is built starting from the pre-oriented unit cell, by subsequently generating images via translation h and twist rotation α. The matrices used for these transformations are denoted by $T = T^{\mathbf{h}}$ and $R = R^{\alpha}$, where $\mathbf{h}$ the translation vector and α the rotation angle with respect to the z-axis, respectively. The first molecule in the tube is obtained by translation $T \cdot \mathbf{x}$ with $\mathbf{h} = (0, -r, 0)$ to all $\mathbf{x} \in \mathcal{X}^0$. We denote this set as $\mathcal{X}^1$.

1. Growth along the **a**-direction: The total number of images generated in this step is n_1. Taking the image $\mathcal{X}^i$ of the previous step, the next image $\mathcal{X}^{i+1}$ is generated by rotation and translation $T \cdot R \cdot \mathbf{x}$ for all $\mathbf{x} \in \mathcal{X}^i$, with $\alpha = \alpha_{\mathrm{a}}$ and $\mathbf{h} = (0, 0, -h_{\mathrm{a}})$. This constitutes the basic helix along the **a**-direction on the tube.

2. Growth along the **b**-direction: Next, this basic helix is copied along the **b**-direction. Starting from each of the n_1 images $\mathcal{X}^i$ $(i = 1, ..., n_1)$ that have been grown along the **a**-direction, a new image $\mathcal{X}^{i+n_1}$ is generated by rotation and translation, *i.e.* $T \cdot R \cdot \mathbf{x}$, for all $\mathbf{x} \in \mathcal{X}^i$ $(i = 1, ..., n_1)$, for a fixed angle $\alpha = -\alpha_{\mathrm{b}}$ and vector $\mathbf{h} = (0, 0, h_{\mathrm{b}})$. This process constitutes two helices on the tube. The same procedure is then applied in an iterative fashion to generate new helices by rotation and translation, with $\mathcal{X}^{i+j\cdot n_1}$ being imaged in $\mathcal{X}^{i+(j+1)\cdot n_1}$ for $i = 1, ..., n_1$ and $j \in \mathbb{N}$. By construction, $\mathcal{X}^1$ and $\mathcal{X}^{n_1 \cdot n_2}$ relate to positions in neighboring unit cells on the lattice, and the total length of the helical assembly can be tuned by the number of helix copies $N_{\mathrm{duplicates}}$ along the **b**-direction. Finally, this assembly is truncated at the bottom and top to provide a cylinder of a predefined length.

A geometrical illustration of 2D growth in this algorithm can be found in Figure 5.2 for $n_1 = 30$ and $n_2 = 10$ with $N_{\mathrm{duplicates}} = 12$. Indeed, a closed tube structure is formed.

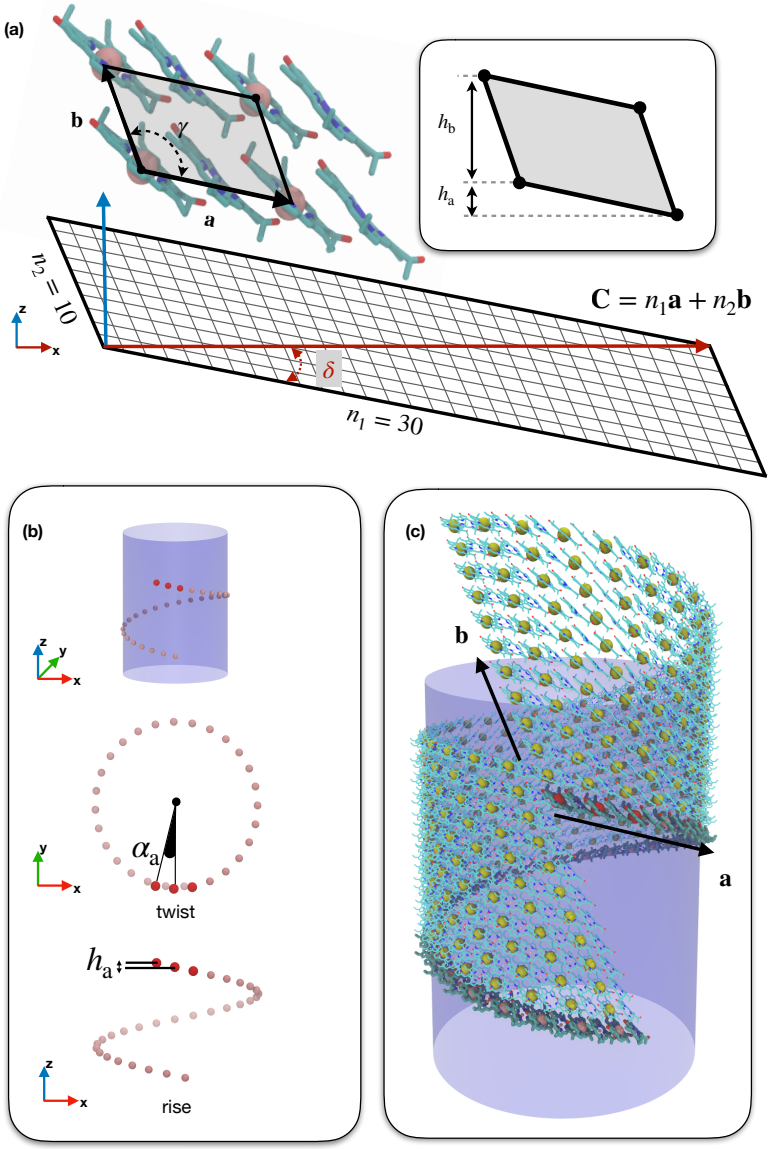

Figure 5.2: Illustration of the tube packing algorithm for the $n_1 = 30$, $n_2 = 10$ case. (a) The chiral lattice and a properly oriented *syn-anti* dimer packing unit. The inset is a 2D illustration of the rise of helices along **a** and **b** directions. (b) Illustration of twist and rise for the helix along the **a**-direction in 3D. (c) The growth along **a** and **b** directions in 3D. The molecules belonging to the basis helix along **a**-direction are shown by dark colors. The molecules further duplicated along the **b**-direction are shown in light colors and their Mg^{2+} are shown in yellow color. The overall structure has 12 basis helices, and it can be treated as a 30-start helix in terms of the helices along **b**-direction.

5.2.3. An Entire Family of Chlorosomal Tubes

Besides curving/rolling direction, the tube chirality is determined by the chiral angle δ, which is the angle between the rolling vector and a reference lattice vector, see Figure 5.3a. we note again that the complete range of δ runs between 0 to 180°, and that we assembled tubes spanning this range, with a resolution of 5 °, using the protocol described above. In line with the observations for all spontaneously formed curvature, we select a curving direction that relates to *syn* tails that are located in the inner side of the tube, see Chapter 2.

To relate to actual chlorosome dimensions, we pre-assembled long tubes with a diameter of 15 nm. Both theoretical and computational studies have pointed towards a length dependence of the optical spectra, particularly in the signature of the CD spectra for shorter tubes,[35,80] but we observed no signature change above 60 nm, see Chapter 3, so we also considered 60 nm tubes in our current analysis. For each chiral angle, a tube composed of roughly half a million atoms was positioned in the center of a sufficiently large simulation volume in order to avoid interactions with periodic images. In the stage of unrestrained MD simulations, tube structures were simulated for 5 ns at 50 K and sequentially another 5 ns at 300 K.

Somewhat to our surprise, we found that all our pre-assembled tubes are very stable, see the extracted structural information in the supporting information file.[1] Moreover, as before, we found that rotations of individual molecules previously identified in curved sheets, see Chapter 2, are conserved when they are closely packed into a tube. This led us to the conclusion that both the local structural characteristics are rather indifferent to the overall tube chirality δ.

To more generally discriminate between different types of helical structures, we may consider $|n_1| + |n_2|$ setting the ratio between the size of composing unit and the size of helical structure, as well as its local curvature. As in our chlorosome structures, with large values of $|n_1| + |n_2|$ and small local curvature, the local packing environment for the composing unit is similar to the planar situation; thus, the dependence on chirality is missing. On the contrary, for structures with small values of $|n_1|+|n_2|$, *e.g.* filaments and protein microtubules, the penalty of changing chirality may be high for the frustrated interactions

[1] File chiral-tubes-structure-summary.csv in chapter_5 folder https://github.com/xinmeng2015/chlorosome_phd_thesis or https://doi.org/10.5281/zenodo.3674742

between composing units.

5.2.4. Chirality versus Optical Response

Finally, we consider the absorption, LD and CD spectra for all tubes in the full range based on the corresponding Frenkel exciton Hamiltonian, in which electronic couplings between pigments are derived from the molecular transition dipole, see more details in Chapter 3. As usual, calculated (stick) spectra were broadened via a convolution with a Gaussian, which mimics experimental broadening due to heterogeneity. In the spectral plots, we show spectra for a range of Gaussian filters, with FWHM values ranging from 10 to 350 cm^{-1}. The supporting information file [1] contains all spectral plots. For instance, for the case $\delta = 5°$, spectral plots are named as 5-absorption.pdf, 5-ld.pdf and 5-cd.pdf. To effectively characterize spectra, we have defined and used different measures for the spectral features. $\Delta\lambda = \lambda_m - \lambda_0$ for absorption spectra, where λ_m is the absorption peak position and λ_0 is the monomer excitation energy. $f_{ld} = (S_+ - S_-)/(S_+ - S_-)$ for LD spectra, where S_+ and S_- are the integrated area of the positive and negative bands of the LD spectrum respectively. Positive/negative f_{ld} indicates that the corresponding structure has a stronger/weaker absorption along the tube axis than that orthogonal to the tube axis. There are four types of psi-shapes for CD spectra: $-/+$, $+/-$, $-/+/-$ and $+/-/+$.

Figure 5.3 shows spectral features for all δ, enabling us to group structures into categories with equivalent optical spectra features. Clearly, the variability or sensitivity of the optical spectra to supramolecular chirality follows the order: absorption < LD < CD. From the results for absorption, see Figure 5.3b, an equivalent red-shift $\Delta\lambda \approx 60$ nm can be seen for all δ, which simply demonstrates that they all belong to the class of J-aggregates.[138] This result indicates that the Q_y absorption band of chlorosomes is mainly determined by the local *syn-anti* packing, with no significant dependence on particular tube chirality. For LD and CD, a clear role of the tube chirality is observed. For LD, see Figure 5.3c, the changing sign of f_{ld} divides the δ range into *three* separate domains: upon increasing δ from 0° to 175°, f_{ld} changes from

[1] File spectra-plots.zip in `chapter_5` folder at https://github.com/xinmeng2015/chlorosome_phd_thesis or https://doi.org/10.5281/zenodo.3674742

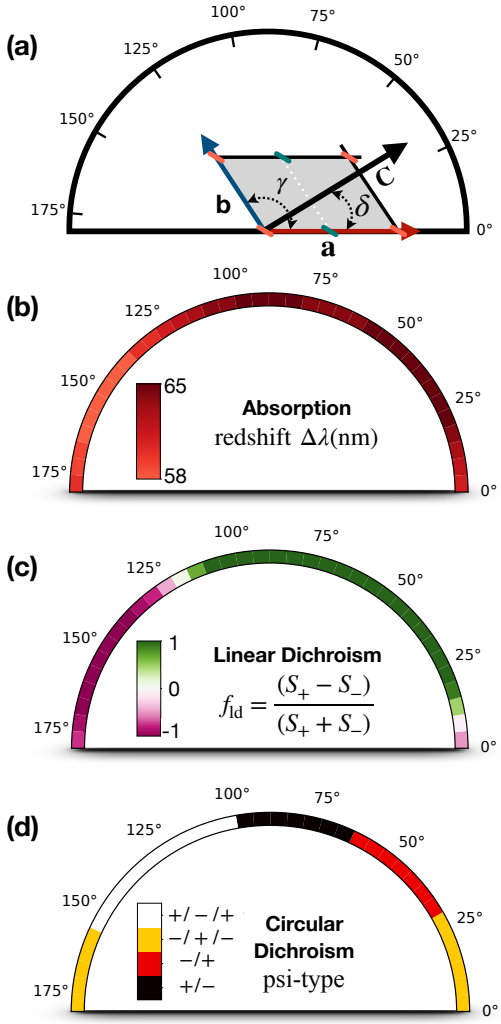

Figure 5.3: (a) Schematics of the 2D helical lattice composed of *syn-anti* packing units and the chiral angle δ. The polar axis is defined according to the δ. (b) A polar plot of spectral features for absorption, LD and CD as a function of δ. The resolution of δ is 5°. For all considered δ tube structures, spectral signatures are identified from spectra that were broadened using a Gaussian kernel with FWHM equal to 200 cm^{-1}, see all the plots in supporting information (spectra-plots.zip).

negative to positive, and then to negative again. Since $f_{\mathrm{ld}} \approx 1$ is observed in all experimental LD spectra, it narrows down the possible range to $[15°, 110°]$. As shown in Figure 5.3d, the CD spectrum is much more sensitive to chirality and *five* separate domains can be identified. In particular, our results show that the mixed-type CD spectra, for instance, the $-/+/-$ type frequently identified for chlorosomes, can originate from a single tube with a well-defined chirality, instead of being the result of stemming from separate structures with opposing chirality. As suggested earlier, it is well known that the structure of chlorosomes depends on the species of bacteria and the specific growth condition. Our results can rationalize why different types of CD spectra are observed experimentally.

Our finding elucidates the relation between CD spectra and the underline tube structure characterized by δ quantitatively. It clearly shows that a transition of the CD spectra signature is consistent with a slight variation of δ, which may well be a result of specific growing conditions; for instance, going from 25° to 30 °, the psi-type CD signal changes from $-/+/-$ to $-/+$. We note that reversing the curving direction will reverse the tube chirality. As shown in Chapter 3, it will simply switch the sign of CD spectra and has little influence on the absorption and LD spectra.

5.3. Conclusions

Calculated optical spectra for chlorosomes and other inspired large TMA structures systems have been reported before, but only based on idealized structural models and specific chiral angles. Thus far, no attention has been given to deriving a systematic relation between tube chirality and optical properties. One of the challenges involved is to obtain realistic atomistic tube structures with prescribed or customized tube chirality. In the present work, we propose such a protocol, based on an in-house tube packing code and a series of relaxation simulations. We employed this protocol to generate realistic atomistic tube structures with a resolution of 5° in the whole range of [0, 180).

Access to a complete set of chiral tube structures allows us to systematically study their properties by computational means, ranging from diffractive, mechanical, optical, or magnetic. In this work, we focus on the optical properties,

in particular the absorption, LD, and CD spectra. Constituting a direct relation between the signature of the optical spectra and their chirality (as encoded in the chiral angle δ) represents a new step towards compiling a handbook for optical spectra measurements of chlorosomes. Implementing further improvements is straightforward, for instance, in terms of the accuracy of the MD force field and the electronic coupling method used to construct the Frenkel Hamiltonian. This first step proposes a practical way to study the role of supramolecular/tube chirality in the structural and functional properties of chlorosomes, as well as other large size tube molecular aggregates.